LES on wind turbines by comparison of Vortex Particle Method and Finite Volume Method codes

Maëlenn Roperch, Venkata Hari Charan Mulakaloori, Pierre Bénard, Grégory Pinon

Journal of Physics: Conference Series **2767** (2024) 092038 doi:10.1088/1742-6596/2767/9/092038

LES on wind turbines by comparison of Vortex Particle Method and Finite Volume Method codes

M Roperch[1], V H C Mulakaloori[2], P Bénard[2] and G Pinon[1]

[1] Laboratoire Ondes et Milieux Complexes, Normandie Univ., UNILEHAVRE, Le Havre, France

[2] CORIA, Normandie Univ., INSA Rouen, UNIROUEN, CNRS, Rouen 76000, France

E-mail: pierre.benard@coria.fr; gregory.pinon@univ-lehavre.fr

Abstract. The aim of this paper is to compare two different computational methods that analyse the flow around wind turbine using Large-Eddy-Simulations (LES). The first method uses a three-dimensional unsteady Lagrangian Vortex Particle method (VP) associated to a lifting-line (LL) approach providing radial loads, integrated thrust and power coefficients, circulations and angle of attack across the turbine blades. The second method solves the incompressible Navier-Stokes equations with the classical Finite Volume (FV) method coupled to the Actuator Line (AL) method to model the rotor blades. Both methods are compared by means of a benchmark consisting in a single full-scale NREL5MW wind turbine and the results are thus compared to Martínez-Tossas et al (2018). The comparisons involve loads, angle of attack and velocity along the blade. Wakes downstream of the turbine are analysed via the evolution of flow fields as mean velocity and vorticity. Results are found to be in good agreement with the verification case. A comparison is also performed on the evaluation of the numerical cost, precision and efficiency of both computational methods.

1. Introduction

Improvement of wind power by understanding its flow physics is still a challenge for the wind energy community [1]. It requires extensive experimental resources or high-fidelity numerical codes to capture these wide range of flow scales involving multi-physics. Following this continuous increase in trend of the High Performance Computing capabilities a variety of numerical approaches are under active development [2, 3] . Nevertheless, such methods remain very expensive and trade offs must be made between accuracy and cost. Moreover, reliability of numerical results are essential for confidence in the analysis. Dedicated benchmark cases have been designed over the last decades to assess the quality of the numerical codes [4, 5].

This paper aims to compare two high-fidelity Large-Eddy Simulation (LES) approaches on an existing benchmark [4] and assess their precision-cost performance: a Lagrangian Vortex Particle method (VP) and a classical Finite Volume (FV) method. This simple benchmark consists in a single full-scale wind turbine configuration subjected to an uniform inflow. Obtained results are first compared against benchmark results [4] assuring a good accuracy of each methodology. Then, VP and FV are compared based on the loads, angle of attack as well as velocity along the blade, in addition to turbine wake quantities. Computational cost and efficiency between methods is also analysed, in comparison with the accuracy of the obtained results.

Section 2 presents the numerical approaches studied in this work, as well as the benchmark configuration and the associated numerical parameters. Section 3 compares both methods in terms of quantitative results and computing performances. Conclusion and perspectives are outlined in Section 4.

2. Numerical methods

2.1. Method 1: LL-VP (Dorothy)

The first solver uses a three-dimensional unsteady Lagrangian VP method [6, 7, 8]. This method is based on the discretisation of the fluid into vorticity carrying particles of vorticity weight $\boldsymbol{\Omega}$. The governing equations for this model are the Navier-Stokes equations for incompressible flows in their discretised velocity-vorticity formulation. These equations are filtered by a filtering operator denoted by $\tilde{\bullet}$ and the continuous formulation is:

$$\frac{\mathrm{D}\tilde{\boldsymbol{\omega}}}{\mathrm{D}t} = \underbrace{(\tilde{\boldsymbol{\omega}} \cdot \boldsymbol{\nabla})\tilde{\boldsymbol{u}}}_{\boldsymbol{S}(\boldsymbol{x},t)} \underbrace{-\boldsymbol{\nabla} \times [\nu_T \boldsymbol{\nabla} \times \tilde{\boldsymbol{\omega}}] + \nu \Delta \tilde{\boldsymbol{\omega}}}_{\boldsymbol{L}(\boldsymbol{x},t)}, \tag{1}$$

where $\boldsymbol{u}$ is the velocity field, $\boldsymbol{\omega} = \boldsymbol{\nabla} \times \boldsymbol{u}$ is the vorticity field and ν is the kinematic viscosity. The fluid domain is discretised into particles. Each particle i is defined by its position $\boldsymbol{X}_i$, vortical weight $\boldsymbol{\Omega}_i$, velocity $\boldsymbol{U}_i$, volume V_i and follows:

$$\begin{aligned} &\frac{\mathrm{d}\boldsymbol{X}_i}{\mathrm{d}t}(t) = \tilde{\boldsymbol{U}}_i(t)\,, \\ &\frac{\mathrm{d}\tilde{\boldsymbol{\Omega}}_i}{\mathrm{d}t}(t) = \tilde{\boldsymbol{S}}(\boldsymbol{X}_i(t),t)V_i + \tilde{\boldsymbol{L}}(\boldsymbol{X}_i(t),t)V_i\,, \\ &\frac{\mathrm{d}V_i}{\mathrm{d}t}(t) = 0\,. \end{aligned} \tag{2}$$

$\boldsymbol{U}_i$ is the sum of the upstream flow velocity and another component coming from a divergence-free vector potential field $\boldsymbol{U}_i^{\psi}$. The core of this Lagrangian method resides in the fact that the velocity $\boldsymbol{U}_i^{\psi}$ is evaluated by the Biot-Savart relation:

$$\boldsymbol{U}_i^{\psi}(t) = \sum_{j=1}^{N} \boldsymbol{K}_{\varepsilon}\left(\boldsymbol{X}_i(t) - \boldsymbol{X}_j(t)\right) \times \boldsymbol{\Omega}_j(t)\,, \tag{3}$$

for which $\boldsymbol{K}_{\varepsilon}(\boldsymbol{x})$ stands for the regularised Biot-Savart kernel [6, 7]. This regularised kernel is basically the convolution product of Biot-Savart kernel with a regularised function $\zeta_{\varepsilon}(\boldsymbol{x})$ of possible different orders. In that respect, the Dorothy code uses two types of algebraic kernels [9], the Moore-Rosenhead (MR) or the Winckelmans-Leonard (WL), which respectively write:

$$\text{MR: } K_{\varepsilon}(\boldsymbol{x}) = \frac{1}{4\pi}\frac{\boldsymbol{x}}{(|\boldsymbol{x}|^2+\varepsilon^2)^{5/2}} \quad \text{or} \quad \text{WL: } K_{\varepsilon}(\boldsymbol{x}) = \frac{1}{4\pi}\frac{\boldsymbol{x}(|\boldsymbol{x}|^2+\frac{5}{2}\varepsilon^2)}{(|\boldsymbol{x}|^2+\varepsilon^2)^{7/2}}, \tag{4}$$

and the associated regularisation functions read:

$$\text{MR: } \zeta_{\varepsilon}(\boldsymbol{x}) = \frac{3}{\varepsilon^3 4\pi}\frac{1}{((\frac{|\boldsymbol{x}|}{\varepsilon})^2+1)^{5/2}} \quad \text{or} \quad \text{WL: } \zeta_{\varepsilon}(\boldsymbol{x}) = \frac{15}{2\varepsilon^3 4\pi}\frac{1}{((\frac{|\boldsymbol{x}|}{\varepsilon})^2+1)^{7/2}}. \tag{5}$$

These functions are depicted in Fig. 1 and will be more in depth detailed and studied in Section 2.4.

Blades are represented via a lifting-line (LL) method [10]. Each blade is represented by a line of points $\boldsymbol{X}_\Gamma$, corresponding to a lifting-line position. At this location, the local circulation Γ_B is evaluated via wing tabulated lift coefficient C_L and local blade chord c such as:

$$\Gamma_B = \frac{1}{2} c |\boldsymbol{u_t}| C_L \,, \tag{6}$$

where $|\boldsymbol{u_t}|$ is the magnitude of the local relative velocity. At each time iteration, new particles are shed following panel-like positioning around each $\boldsymbol{X}_\Gamma$ position. More technical details are given in [10]. Via the knowledge of the local relative velocity $\boldsymbol{u}_t$ and angle of attack, the LL method allows to compute radial loads, circulations, angle of attack and integrated power and thrust coefficient. In that respect, it can be clearly understood that the choice of the regularisation function (Eq. (5)) has an influence on both the load calculation and the wake development, for instance wake velocity profiles. This is further analysed in Sections 2.4 and 3.

2.2. Method 2: AL-FV (YALES2)

The second solver uses the classical FV method, implemented into the YALES2 platform [11] for which high precision is achieved thanks to 4th order space and time numerical schemes [12]. Also, it has shown accuracy when applied to wind turbine simulations [13]. Filtered Navier-Stokes equations for incompressible flow are solved with a prediction-correction method [14] on an Eulerian grid:

$$\begin{aligned} &\nabla \cdot \tilde{\boldsymbol{u}} = 0 \,, \\ &\frac{\partial \tilde{\boldsymbol{u}}}{\partial t} + (\tilde{\boldsymbol{u}} \cdot \boldsymbol{\nabla})\tilde{\boldsymbol{u}} = -\boldsymbol{\nabla}\tilde{P} + \nu \boldsymbol{\nabla}^2 \tilde{\boldsymbol{u}} + \boldsymbol{\nabla} \cdot \tilde{\boldsymbol{\tau}}^M + \boldsymbol{f}, \end{aligned} \tag{7}$$

where P is the reduced pressure field, $\boldsymbol{\tau}^M$ the modeled sub-grid scale stress tensor and $\boldsymbol{f}$ the external body force term. The filtering operator is denoted by $\tilde{\bullet}$.

The wind turbine rotor is modeled using the Actuator Line (AL) method [3], where each turbine blade is represented by a virtual line rotating with a prescribed motion. Lift and drag forces are computed on each point discretising the line via the airfoil theory and then projected on the Eulerian grid via a mollification kernel. The later is a Gaussian regularisation function η of equation:

$$\eta(\boldsymbol{x_p}) = \frac{1}{\varepsilon^3 \pi^{3/2}} \exp\left[-\left(\frac{|\boldsymbol{x_p}|}{\varepsilon} \right)^2 \right] , \tag{8}$$

where $\boldsymbol{x_p}$ is the distance between an actuator point and a mesh node. ε is the regularisation parameter defining the spread of the kernel. Its influence on the regularisation function η is represented in Fig. 1. One of the objectives of the present paper is to assess and understand the role of ε-value in both representations (LL or AL) and its influence on the obtained results, both in terms of load and wake evaluation.

2.3. Numerical set-up

The benchmark case [4] consists of a single NREL5MW turbine [15] of diameter $D = 126\,\mathrm{m}$ and rotation speed $\Omega = 9.155\,\mathrm{r.p.m.}$ submitted to a uniform laminar inflow of velocity $U_\infty = 8\,\mathrm{m.s^{-1}}$ in a $24D \times 6D \times 6D$ domain, with the turbine center located $3D$ downstream of the inlet.

This case has been studied by 4 teams in the original article [4], namely KUL, NREL, JHU and DTU in this work, but others publications refer to this case [16, 17]. All the studies use a different numerical approach, from Finite Difference to Spectral Methods, coupled with an AL. To the authors knowledge, this case has never been studied using a VP method coupled to LL.

The original benchmark uses an homogeneous cartesian grid of $\Delta x \approx 2\,\mathrm{m}$, while other publications use heteregenous grid but with a similar mesh size in the zone of interest, i.e.

Table 1: Code parameters and associated relevant information. *Computation only performed up to 12D behind the turbine.

YALES2 (Y2)	ε_{Y2} [m]	dr [m]	N_{sec}	Δx [m]	Δt [s]	nb nodes	T_{tot} [s]	CPU/T_{tot} [h.core/s]
	10	0.96	64	1.96	0.15	227×10^6	1955.5	14.4
	3.84	0.96	64	1.96	0.15	227×10^6	1955.5	14.4
DOROT. (MR)	ε_{MR} [m]	dr [m]	N_{sec}	Δx [m]	Δt [s]	nb part	T_{tot} [s]	CPU/T_{tot} [h.core/s]
	10	1.92	32	6.67	0.15	410 000	1796	48.5
	3.84*	1.92	32	2.56	0.059	4 800 000	300	236.5
	2.88*	1.92	32	1.92	0.032	5 800 000	250	390.0
DOROT. (WL)	ε_{WL} [m]	dr [m]	N_{sec}	Δx [m]	Δt [s]	nb part	T_{tot} [s]	CPU/T_{tot} [h.core/s]
	10*	1.92	32	6.67	0.15	200 000	1796	30.0
	3.84*	1.92	32	2.56	0.059	4 600 000	400	229.5

the rotor and its wake, while the rotor is almost always modelled with the AL using a spreading kernel size of $\varepsilon = 10\,\mathrm{m}$. All studies use the sub-grid scale turbulent fluxes are modelled with the Smagorinsky model. Contrary to the original publication, time averaging are based on a duration of 65.5 s, i.e. 10 turbine rotations.

2.4. Codes parametrization

The aim of the paper being a cross-comparison of both LL-VP and AL-FV methods, a clear definition of most important parameters of each formulation is given in Table 1 together with other relevant information, such as computational cost. Generally speaking, both codes highlight similarities and differences in parameters which will be detailed in the following.

As for the similarities, both code have a blade of length L_{blade}, which is discretised into N_{sec} elements (being either AL or LL points). In that respect, a blade discretisation can be defined as $dr = L_{blade}/N_{sec}$. Also, both codes have a fluid discretisation, being either the fluid cell size Δx for YALES2 or the fluid inter-particle spacing also denoted Δx for Dorothy. The Δx value will have an influence on the number of cells for YALES2 and on the number of particles for Dorothy, and hence a large influence on the computational cost of each simulation. YALES2 computations use the homogeneous Cartesian grid as defined in the original benchmark [4] while the fluid inter-particle spacing for Dorothy depends on the regularisation parameter ε (see below). Therefore, all of these parameters and related CPU times are indicated in Table 1. For Dorothy, being a Lagrangian code, no boundary is defined and the turbine is basically positioned at the origin of space $(0, 0, 0)$. For some computations and to avoid too high a computational cost, particles are artificially but smoothly dissipated at a rate of $50\%/s$ for $x > 12D$.

Concerning the differences, the major variation resides in the definition of the ε parameter. In AL-FV formulation with YALES2, ε_{Y2} is used to project the loads onto the grid. The fluid velocity upstream is interpolated onto the blades and the computed forces are projected from the modelled solid blades to the fluid mesh via the Gaussian kernel (Eq. (8)) of size ε_{Y2}. The quality of the wake is influenced by both the size of the mesh Δx, which influences the diffusion and the dissipation of the wake, and ε_{Y2}, which describes the spreading of force projected onto the fluid mesh. As illustrating by Fig. 5, this spreading directly influences the size of the blade-created coherent fluid structures: from fine helical tip and root vorticies with low ε_{Y2}-values

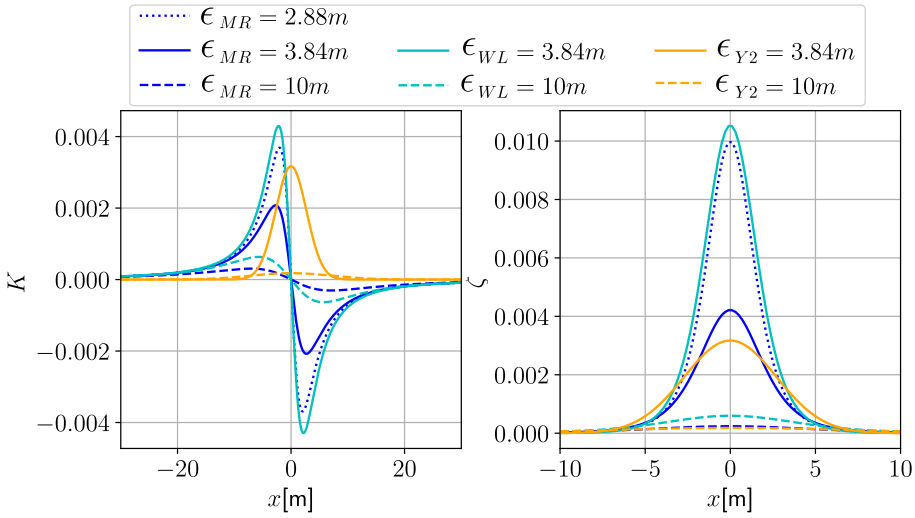

Figure 1: Regularised kernel (left) and regularisation function (right) for each computed case.

to cylindrical vorticity sheet with higher ones. This process inevitably impacts on the wake development downstream the turbine.

For LL-VP formulation with Dorothy, the regularisation parameter ε_{MR} or ε_{WL} has a stronger influence, both for the blade load calculation and the wake evaluation. In fact, and contrary to YALES2, ε is used all over the domain and is not restricted to a volume close to the blade. For the flow calculation, this regularisation parameter being used to avoid singularity in the velocity evaluation (see Eq. (3)), ε is chosen to "overlap" the inter-particle's distance and $\varepsilon = 1.5\Delta x$ is usually chosen [7]. Therefore, there is a clear limitation: ε and Δx cannot be chosen completely independently. Also, owing to the shedding process of particles at the blade, another limitation exists that is $dr \approx \Delta x$. As a consequence, N_{sec} cannot be chosen too independently neither as too high a value of N_{sec} will give a very small value of dr, leading to a similar value of Δx (very refined discretisation), hence leading to a very high number of particles and associated simulation cost.

As a consequence, a trade-off needed to be made with respect to the benchmark definition parameters of Martinez-Tossas *et al.* [4] to account for these limitations. In the rest of the paper, a systematic comparison of YALES2 results with Dorothy ones (both with MR or WL kernels) is performed by comparing the results of similar value of ε for both formulation. In that respect, two important values of $\varepsilon = 10\,\mathrm{m}$ and $\varepsilon = 3.84\,\mathrm{m}$ are chosen to match respectively the value of $\varepsilon = 10\,\mathrm{m}$ as in the benchmark computations [4] and $\varepsilon = 3.84\,\mathrm{m}$ being the lowest value possible for YALES2 having the same mesh size as Martinez-Tossas benchmark and keeping the stability of the AL method. Lower ε values could have also been possible with AL-FV method but this requires a lower mesh size, a higher number of cells leading to increased computational times. The values of ε being similar in Table 1, but the regularised functions or kernels being different and there role being very different, a basic comparison is not directly possible based on the plot of these functions as depicted in Fig. 1. Actually, the Biot-Savart Kernel $\boldsymbol{K}_\varepsilon$ being applied on the velocity calculation of Eq. (3) is asymmetric, which is not the case for $\eta(\boldsymbol{x_p})$ (Eq. (8)) applied to the force. As a matter of comparison, ζ_ε (Eq. (5)) has a radial symmetry property but does not have a similar role neither. The presented graphs of Fig. 1 are plotted for each functions (ζ_ε, $\boldsymbol{K}_\varepsilon$ and η) with the corresponding value of ε. Non-dimensional plots could have been considered but would have been more complicated to analyse as the dimensional aspect of the function been different, it would have hidden some of its influence.

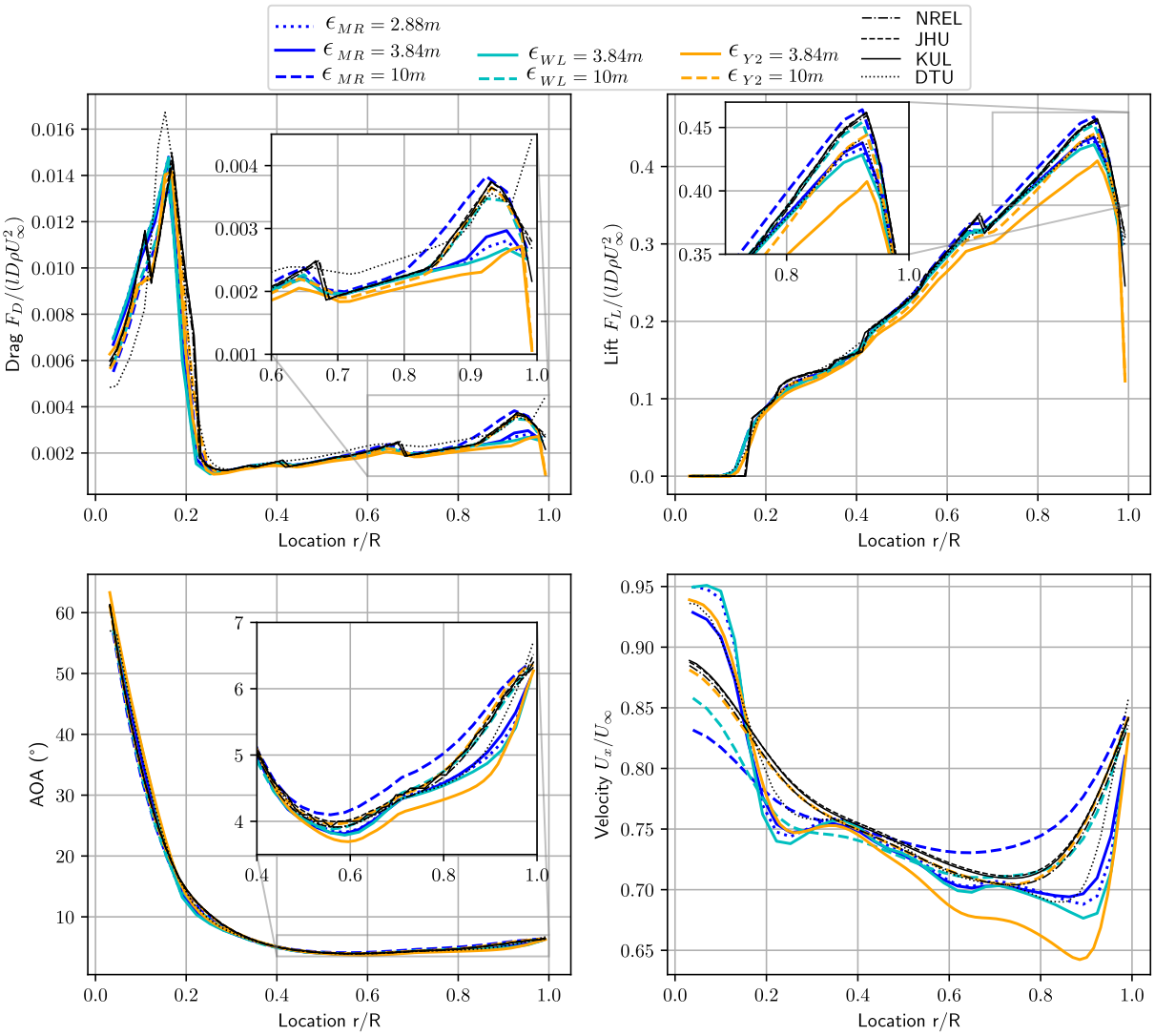

Figure 2: Spanwise evolution of radial forces, angle of attack and velocity comparison for all cases, compared to results from [4].

3. Comparison

3.1. Quantities along the blade

Firstly, fluid and blade related quantities are compared between codes for each case presented in Table 1. Figure 2 presents the blade spanwise evolution of time-averaged Angle Of Attack (AOA), streamwise fluid velocity U_x, drag F_D and lift F_L forces on blade. As a general first comment, all results look similar and accurate with respect to the benchmark results [4] for the AOA, lift and drag forces. Only the upstream blade velocity U_x shows some noticeable discrepancy.

More into the details, and starting with the AOA, $\varepsilon_{Y2} = 10\,\text{m}$, $\varepsilon_{WL} = 10\,\text{m}$ and JHU, NREL & KUL results (all at $\varepsilon = 10\,\text{m}$) superimpose, even looking at the sub-plot between $0.4 \leq r/R \leq 1$. As a consequence, all related quantities (U_x, F_D and F_L) also quasi superimpose. The case of $\varepsilon_{MR} = 10\,\text{m}$ is a little unique and does not really compare with other results. It is worth mentioning here that this kernel is known to be at very low order and tends to smooth the results. On the contrary, $\varepsilon_{Y2} = 3.84\,\text{m}$, $\varepsilon_{WL} = 3.84\,\text{m}$ and even $\varepsilon_{MR} = 3.84\,\text{m}$ show similar results both

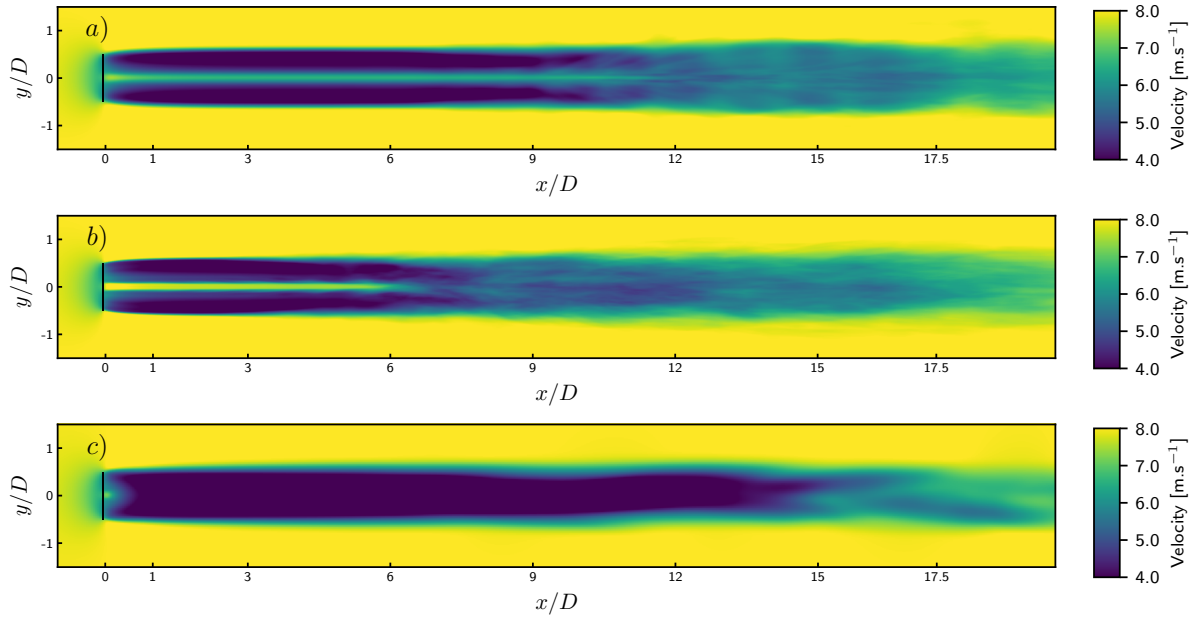

Figure 3: Time-averaged velocity field in $x-y$ plane for (a) with $\varepsilon_{Y2} = 10$m, (b) with $\varepsilon_{Y2} = 3.84$m and (c) is $\varepsilon_{MR} = 10$m.

for AOA, velocity (U_x) and loads (F_D and F_L). These results are quite different from those of JHU, NREL & KUL but very similar to those of DTU. As a consequence, the obtained results may not be considered as erroneous but must be explained by some physical interpretation. As a matter of fact, it is really surprising to see how these results superimpose well with DTU on U_x/U_∞, especially for $r/R \leq 0.2$ and $r/R \geq 0.75$. Finally, the presented results for $\varepsilon_{MR} = 2.88\,\text{m}$ are always comprised between those of $\varepsilon_{MR} = 3.84\,\text{m}$ and $\varepsilon_{WL} = 3.84\,\text{m}$. In that sense, it could be seen as further converged results, in terms of spatial convergence.

As a matter of numerical interpretation, the ε-parameter seems to have a similar behaviour in AL and LL methods: Dorothy LL-VP, YALES2 AL-FV and JHU, NREL & KUL behave very similarly with $\varepsilon = 10\,\text{m}$. JHU, NREL & KUL results do not exist for $\varepsilon = 3.84\,\text{m}$ but Dorothy LL-VP and YALES2 AL-FV behave similarly for such value.

To conclude, the ε-parameter has a large influence on the load evaluation, even more important than the mesh definition Δx and the blade discretisation dr. Whatever the underlying fluid solver is, AL representations behave very similarly for a given ε-value. The role of ε in the Lagrangian LL-VP formulation show similar tendency to those of AL representations even though it is intrinsically different in term of numerical definition/implementation.

3.2. Wake quantities

The methods comparison is now continued regarding their influence on obtained wake velocities. Time-averaged velocity and instantaneous vorticity fields downstream of the wind turbine are presented in Fig. 3 and Fig. 5 respectively. To enable better comparison, averaged velocity profiles are also depicted in Fig. 4 for different positions in the wake, from very close to the rotor plane to $9D$ downstream. For the plots of Fig. 3, similar global trends and average velocity deficit ($\approx 0.4\,m/s$) of the wakes are observed whatever the case. However, discrepancies are also well noticeable: first, an important bypass velocity is observable at the hub level for both computation using YALES2 whereas this bypass flow is only noticeable for a very short length with Dorothy computation. Second, and apart from this bypass flow, the global wake shape of $\varepsilon_{Y2} = 10\,\text{m}$ is similar to the one of $\varepsilon_{MR} = 10\,\text{m}$ especially from $x/D \geq 10$.

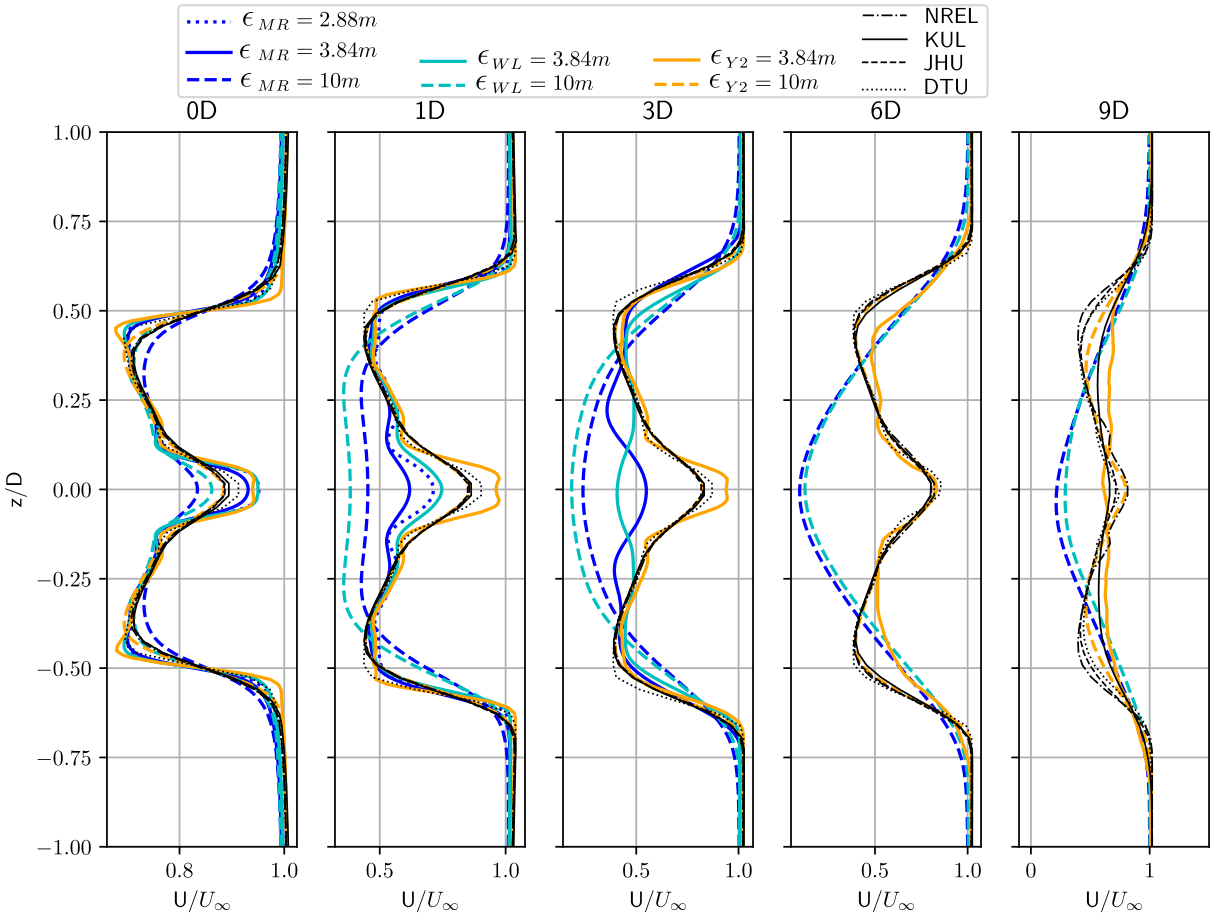

Figure 4: Mean velocity comparison in the wake for all codes.

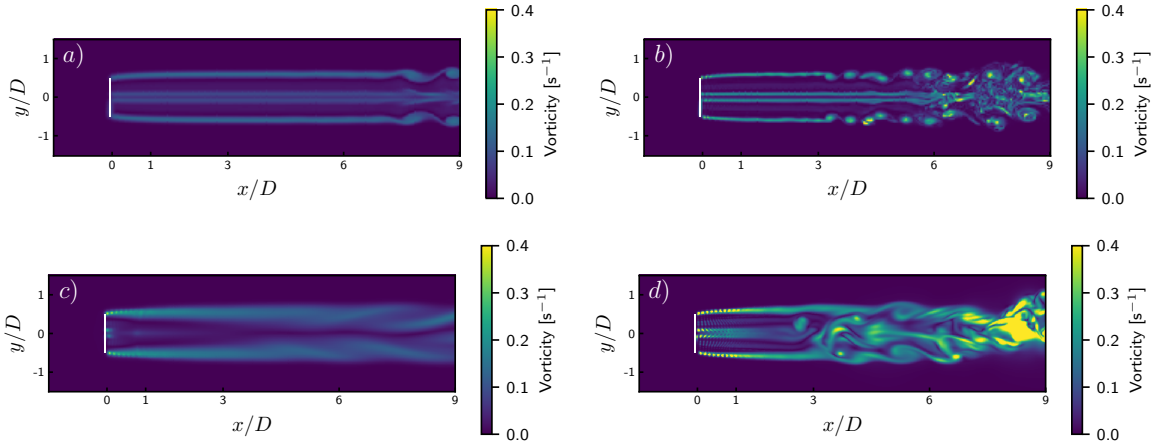

Figure 5: Norm of instantaneous vorticity field in $x-y$ plane for (a) $\varepsilon_{Y2} = 10$m, (b) $\varepsilon_{Y2} = 3.84$m, (c) $\varepsilon_{WL} = 10$m and (d) $\varepsilon_{WL} = 3.84$m.

As a matter of further comparison, wake velocity profiles of Fig. 4 can be compared for all codes and nearly all parameters of Table 1. The first and important result from this plot is that $\varepsilon_{Y2} = 10\,\mathrm{m}$ results nearly always superimpose with those of JHU, NREL & KUL, and also with DTU ones in some respect up to nearly $9D$ downstream of the turbine. Therefore, for

averaged velocity profiles, $\varepsilon_{Y2} = 10\,\mathrm{m}$ could be viewed as a reference case with respect to the benchmark case [4]. For the lower value of $\varepsilon_{Y2} = 3.84\,\mathrm{m}$, two observations can be drawn from YALES2 results: first the bypass flow at the hub height is further intensified with larger values up to $x/D \leq 3$ or even $x/D \geq 6$ to a smaller extent. Then, for the velocity profile presented at $x/D = 9$, a reversed tendency starts to be observable as if the wake was taking a Gaussian shape, typical of far-wake structure. Anyway, YALES2 results are very similar to those of the benchmark case [4] both with $\varepsilon_{Y2} = 10\,\mathrm{m}$ and $\varepsilon_{Y2} = 3.84\,\mathrm{m}$.

For Dorothy results, the situation is a little different and for several reasons. First, only the results of $\varepsilon_{MR} = 10\,\mathrm{m}$ and $\varepsilon_{WL} = 10\,\mathrm{m}$ are presented up to $9D$ downstream of the turbine because those for lower values of ε were not run on a sufficient duration ($T_{tot} \leq 250 - 400\,s$) to enable correct averaging. In fact, $\varepsilon_{MR} = 3.84\,\mathrm{m}$, $\varepsilon_{WL} = 3.84\,\mathrm{m}$ and even $\varepsilon_{MR} = 2.88\,\mathrm{m}$ are only presented up to $1D$ downstream. Now, from these results, one can clearly observe that both $\varepsilon_{MR} = 10\,\mathrm{m}$ and $\varepsilon_{WL} = 10\,\mathrm{m}$ results are too smoothed in comparison to the benchmark results. This is already slightly observable from $x/D = 0$ and it becomes obvious from $x/D = 1$. The reason for that is that, in Lagrangian Vortex computations, velocity profiles are smoothed according to the regularisation parameter value, that is here $\varepsilon = 10\,\mathrm{m}$ whereas the wake profile for the Eulerian counterparts are smoothed with respect to the cell size, that is here $\Delta x = 2\,\mathrm{m}$. Therefore, decreasing the value to $\varepsilon_{MR} = 3.84\,\mathrm{m}$ only slightly improved the results, as one can see for $x/D = 1$, but insufficiently. Only values of $\varepsilon_{WL} = 3.84\,\mathrm{m}$ with the sharper kernel of Winkelmans-Leonard or $\varepsilon_{MR} = 2.88\,\mathrm{m}$ significantly improve the results from this $x/D = 1$ velocity profile. Unfortunately, averaged velocity profiles for these values of ε could not be evaluated because of the too demanding computational cost for the time being. However, important optimisation work is under progress on this code to try to cope with this and try to catch up the sequential and parallel efficiency of YALES2.

Also, apart for this above mentioned behaviour, Dorothy LL-VP also tends to trigger the wake instability earlier than YALES2 AL-FV. In fact, from Fig. 5, one can see that lowering the ε_{Y2} value from 10 m to 3.84 m triggers the wake instability from $x/D \approx 9$ to $x/D \approx 3$. However, for similar values of ε with Dorothy, this instability seems to be triggered even earlier.

As a matter of partial conclusions, several main findings can be drawn from this wake study: first, YALES2 results seems to be representative of the benchmark codes, at least for the average velocity profiles. Second, the characteristic length scale for Eulerian formulations regarding wake velocity profiles depends on cell discretisation Δx [18] whereas it is still ε for its Lagrangian formulation counterpart, here represented by Dorothy LL-VP. Third, even for the AL-FV code, the smaller the ε is, the earlier the wake instability is triggered [19, 20], which is understandable owing to the different vorticity generation at the blade level. For the LL-VP code, the smaller the ε is, the earlier this wake instability is triggered is also valid. However, wake instability seems to be triggered much earlier in the wake for the LL-VP Dorothy code in comparison with the AL-FV YALES2 code, even for similar values of ε. Finally, and owing to the presented results for Table 1, obtaining averaged results for ε_{MR} or ε_{WL} values similar to those of Δx in AL-FV YALES2 code is currently unaffordable.

4. Conclusions and perspectives

The simulation of a single turbine has been performed on both LL-VP and AL-FV methods. The radial loads follow the trend and almost superimpose on each other, while the differences which arise at a given span-wise location can be attributed to the methodology of codes and the choice of ε-parameter. Even though ε-parameter has a different numerical significance in both approaches, it behaves in a relevant manner for the blade related quantities.

Comparison of mean velocity and instantaneous vorticity fields is also performed to analyse the downstream flow, together with wake velocity profiles. From this study, it comes out that the relevant length scale is still ε for the LL-VP whereas it is the cell size Δx for its AL-FV

counterpart. Also, wake evaluation with the current version of LL-VP code is complicated for the considered discretisation as computations are very CPU intensive whereas it is not the case for the AL-FV code. As the two described methods do not have the same numerical resolution of the fluid, a comparison on computational cost, efficiency of the methods is rapidly presented.

Further studies should be performed upon more various kernel sizes than those presented here in the LL-VP method to ascertain the presented conclusion. Computations with several cell discretisation for the AL-FV code will also be needed to be able to compare this characteristic length with respect to kernel size for LL-VP. Also, an important aspect will be the introduction of ambient turbulence into the domain which can reduce the computational cost for Dorothy and also can stretch the wake longer than $12D$ naturally. Finally, the interaction of wakes of multiple turbines will be very interesting to analyse to be comparable with real life scenarios.

Acknowledgments

This work is supported by the French Agence Nationale de la Recherche (ANR) and the Normandy Region through the Labex program EMC3 (ANR-10-LABX-09-01) and the WILIAM project. Part of this work was performed using computing resources of CRIANN (Normandy, France), as well as computer and storage resources by GENCI at TGCC thanks to the grant A0142A11335 on the supercomputers Joliot Curie's the ROME partition. This work has been initiated during the Extreme CFD Workshop & Hackathon (https://ecfd.coria-cfd.fr).

References

[1] Veers P, Dykes K, Lantz E, Barth S, Bottasso C L, Carlson O, Clifton A, Green J, Green P, Holttinen H, Laird D, Lehtomäki V, Lundquist J K, Manwell J, Marquis M, Meneveau C, Moriarty P, Munduate X, Muskulus M, Naughton J, Pao L, Paquette J, Peinke J, Robertson A, Rodrigo J S, Sempreviva A M, Smith J C, Tuohy A and Wiser R 2019 *Science* **366**(6464)
[2] Martínez Tossas L, Churchfield M and Meneveau C 2015 *Journal of Physics: Conference Series* **625**
[3] Sørensen J N and Shen W Z 2002 *Journal of Fluids Engineering* **124** 393–399
[4] Martínez-Tossas L A, Churchfield M J, Yilmaz A E, Sarlak H, Johnson P L, Sørensen J N, Meyers J and Meneveau C 2018 *Journal of Renewable and Sustainable Energy* **10** 033301
[5] Doubrawa P, Quon E W, Martinez-Tossas L A, Shaler K, Debnath M, Hamilton N, Herges T G, Maniaci D, Kelley C L, Hsieh A S, Blaylock M L, van der Laan P, Andersen S J, Krueger S, Cathelain M, Schlez W, Jonkman J, Branlard E, Steinfeld G, Schmidt S, Blondel F, Lukassen L J and Moriarty P 2020 *Wind Energy* **23**(11) 2027–2055
[6] Pinon G, Mycek P, Germain G and Rivoalen E 2012 *Renewable Energy* **46** 111–126
[7] Cottet G H and Koumoutsakos P D 2000 *Vortex Methods : Theory and Practice* (Cambridge University Press) ISBN 978-0-521-62186-1
[8] Mycek P 2013 *Étude Numérique et Expérimentale Du Comportement d'hydroliennes* Ph.D. thesis Université du Havre
[9] Winckelmans G and Leonard A 1993 *Journal of Computational Physics* **109** 247–273
[10] Dufour M A, Pinon G, Rivoalen E, Blondel F and Germain G 2024 *Wind Energy* **27**
[11] MoureauV 2023 YALES2 CORIA `https://www.coria-cfd.fr/index.php/YALES2` [Accessed: 2023-08-24]
[12] Benard P, Viré A, Moureau V, Lartigue G, Beaudet L, Deglaire P and Bricteux L 2018 *Computers & Fluids* **173** 133–139
[13] Houtin-Mongrolle F, Benard P, Lartigue G and Moureau V 2021 *Journal of Physics: Conference Series* **1934** 012011
[14] Chorin A J 1968 *Mathematics of Computation* **22** 745–762
[15] Jonkman J, Butterfield S, Musial W, Scott G, Jonkman J, Butterfield S, Musial W and Scott G 2009 (February)
[16] Stipa S, Ajay A and Brinkerhoff J
[17] Taschner E, Folkersma M, Martínez-Tossas L A, Verzijlbergh R and van Wingerden J W 2023 (John Wiley and Sons Ltd)
[18] Asmuth H, Olivares-Espinosa H and Ivanell S 2020 *Wind Energy Science* **5** 623–645
[19] Troldborg N 2009 *Actuator Line Modeling of Wind Turbine Wakes* Ph.D. thesis
[20] Hodgson E L, Grinderslev C, Meyer Forsting A R, Troldborg N, Sørensen N N, Sørensen J N and Andersen S J 2022 *Frontiers in Energy Research* **10** 864645